Supporting Information

Fabricating 3D freestanding metamaterials on elastic substrates via the shadow metal-sputtering and plastic deformation

Qiushun Zou, [a,b] Jian Ou-Yang, [a] Xiaoyi She, [a] Yang Shen, [a] and Chongjun Jin*, [a]

[a]State Key Laboratory of Optoelectronic Materials and Technologies, Guangzhou Key Laboratory of Flexible Electronic Materials and Wearable Devices, School of Materials Science and Engineering, Sun Yat-sen University, Guangzhou 510275, China

[b]Faculty of Electrical Engineering and Computer Science, The Research Institute of Advanced Technologies, Key Laboratory of Photoelectric Detecting Materials and Devices of Zhejiang Province, Engineering Research Center for Advanced Infrared Photoelectric Materials and Devices of Zhejiang Province, Ningbo University, Ningbo 315211, China

*(C. Jin) E-mail: jinchjun@mail.sysu.edu.cn

Supplementary figures

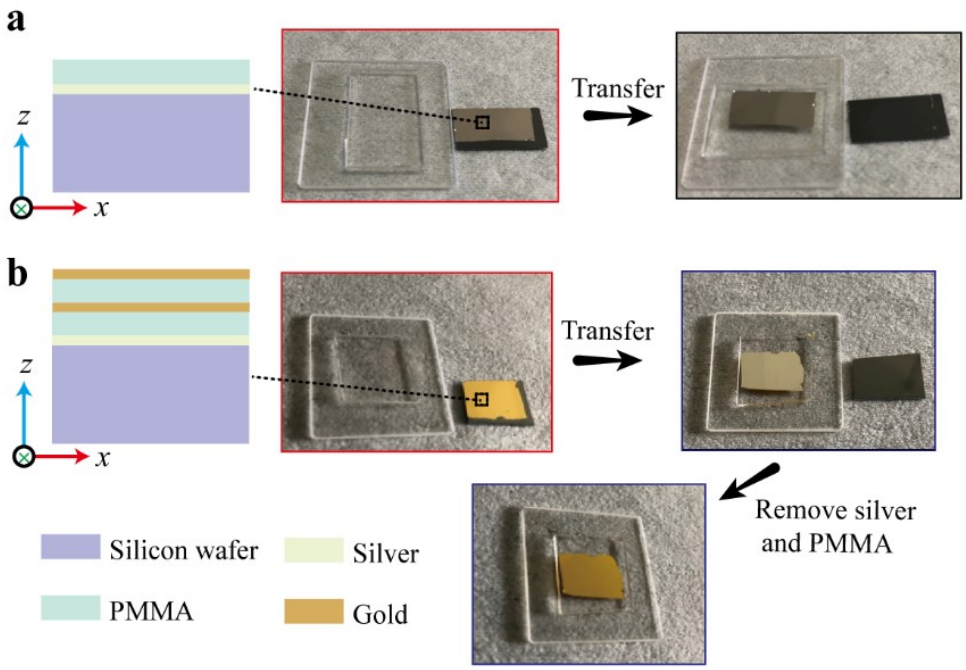

Fig. S1 Photographs of silver-assisted multifilm transfer. (a) A 150 nm silver film with a 793 nm PMMA was perfectly transferred together on a PDMS slab, which was fixed previously on glass. (b) Five films, consisting of silver, PMMA, and gold films, were also perfectly transferred together on a PDMS substrate. The remaining multifilm remains perfect after removing silver and PMMA films in sequence.

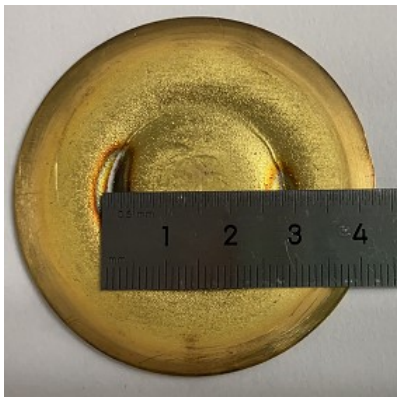

Fig. S2 A photograph of a gold target was used frequently on the magnetron sputter. It was found that the gold target exhibits an etching ring.

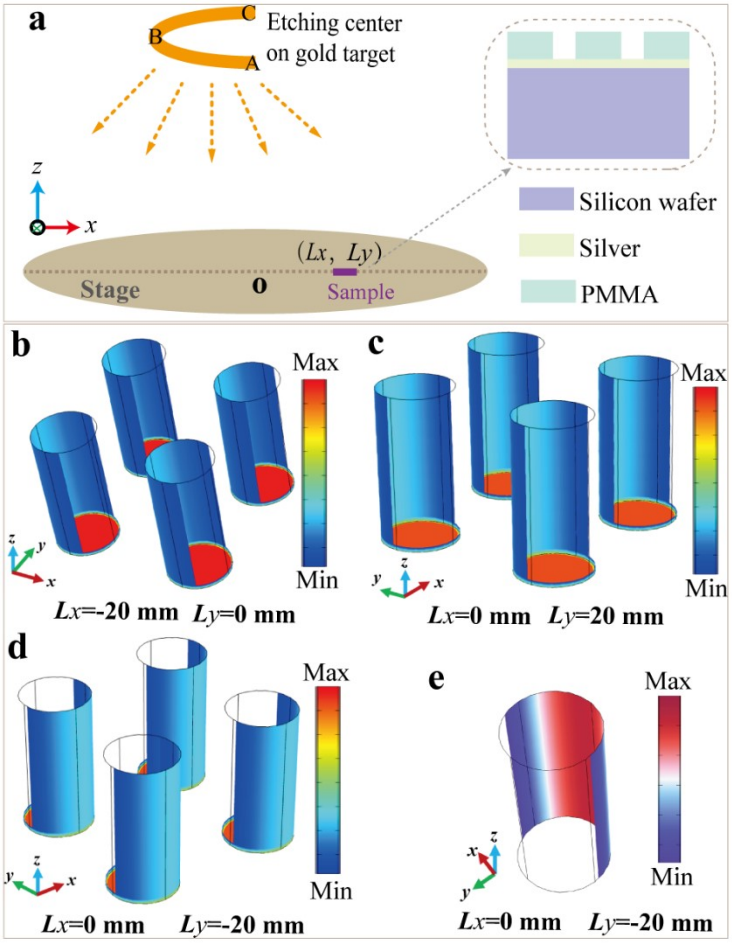

Fig. S3 (a) Schematics of the optical radiation model. The surface exposure intensity reflects the deposited thickness of the gold film. The half-ring source could be regarded as composed of a series of point sources, which are assumed to be radiation uniformly in all directions. The distance between the sample and the center of the object stage is set as *L* (*Lx, Ly*). (b-d) The exposure intensity of cylindrical holes at different positions was also simulated by using the FEM. (e) The exposure intensity of a broken sidewall at a place (*Lx*=0 mm, *Ly*=-20 mm).

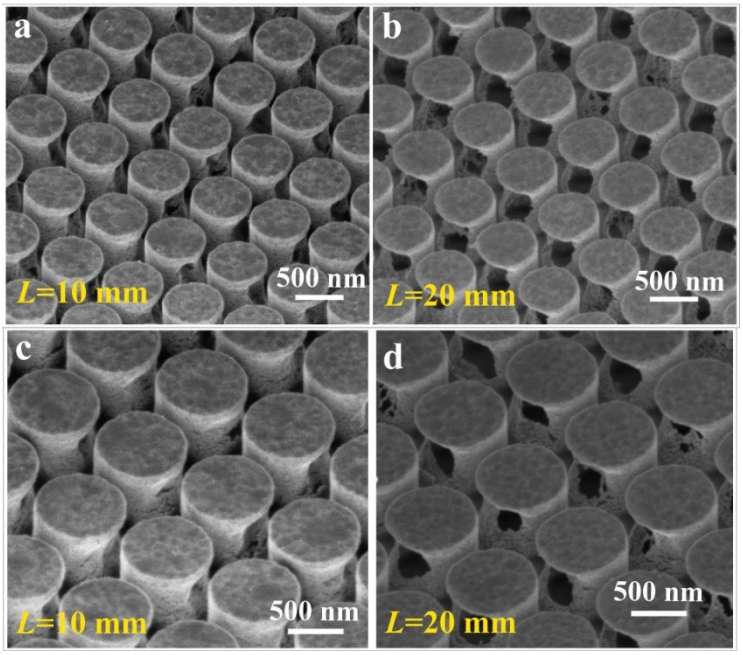

Fig. S4 (a-b) SEM images of fabricating 3D freestanding hollow cylinders (538 nm in diameter, 793 nm in height) under the distance *L* of (a) 10 mm and (b) 20 mm. (c-d) 3D freestanding hollow cylinders (760 nm in diameter, 793 nm in height) at the distance *L* of (c) 10 mm and (d) 20 mm.

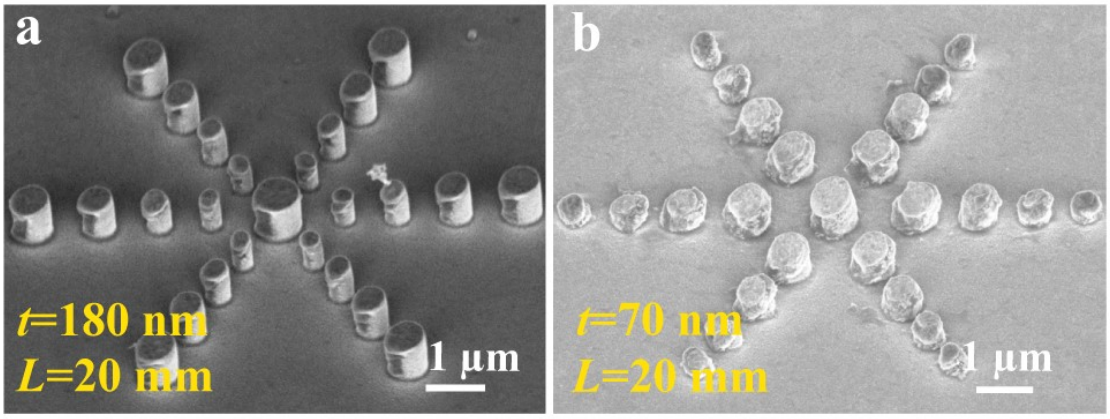

Fig. S5 SEM images of the 793 nm-height hollow cylinders with diameters varying from 230 to 680 nm. The deposited thickness is (a) 180 nm and (b) 70 nm, respectively. The sputtering samples are located at *L*=20 mm.

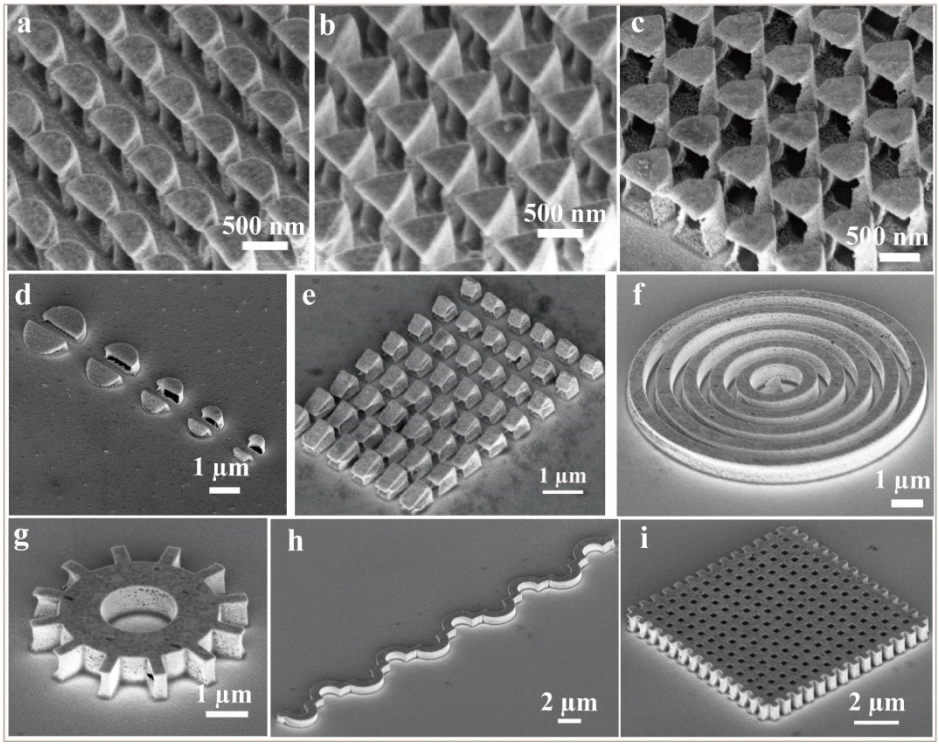

Fig. S6 SEM images of various 3D freestanding hollow structures, such as (a) half-cylinder array, (b) triangular prism array, and (c) pentagonal prism array. (d) Breaking half-cylinders with diameters varying from 600 nm to 1.62 µm. (e) Slanted cuboids with different lengths of sides. (f) The bull's eye. (g) Gear. (h) Long-chain structure. (i) porous structure.

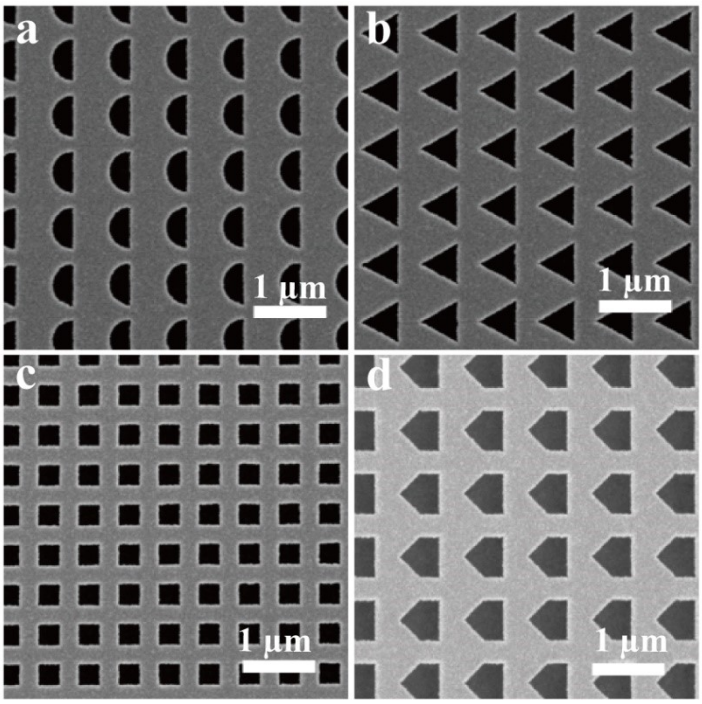

Fig. S7 SEM images of the planar structures to transfer 3D structures that are shown in Figure 2(a-d).

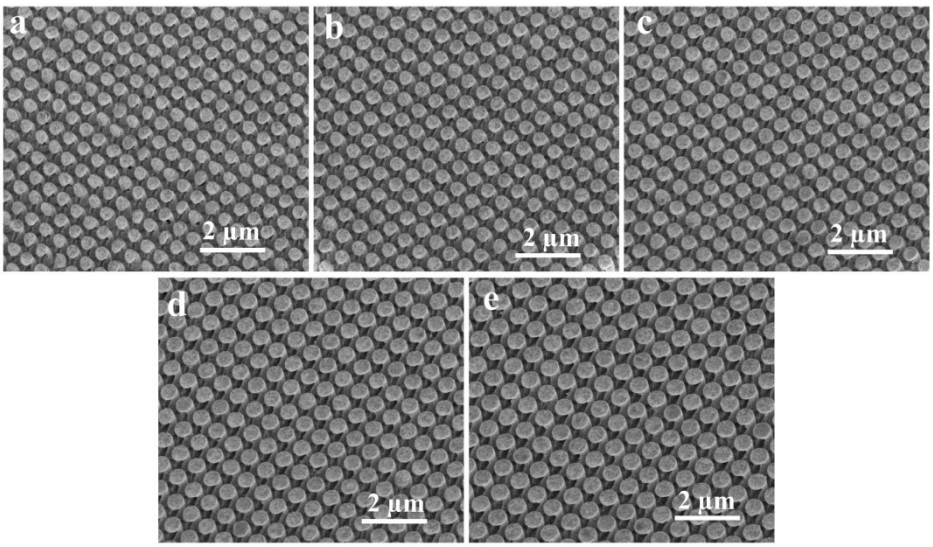

Fig. S8 (a-e) SEM images of the large area of the 3D freestanding cylinder array corresponding to Figure 3c-g.

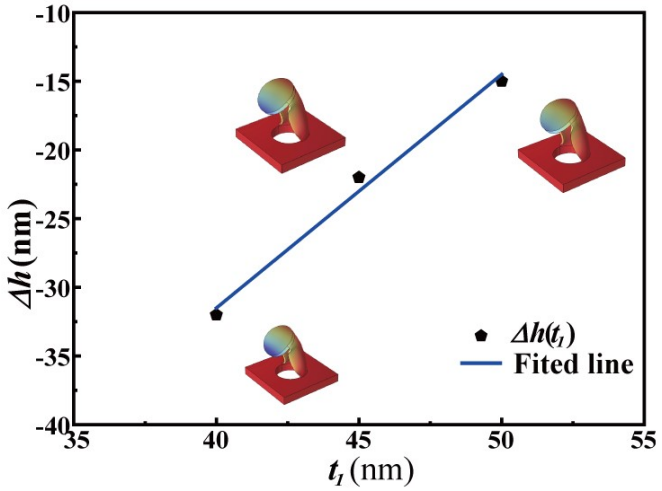

Fig. S9 The height change Δh as a function of the thickness t_1 of the sidewall. The three insets represent the deformed structures of the cylinders with thicknesses varying from 40 to 50 nm.

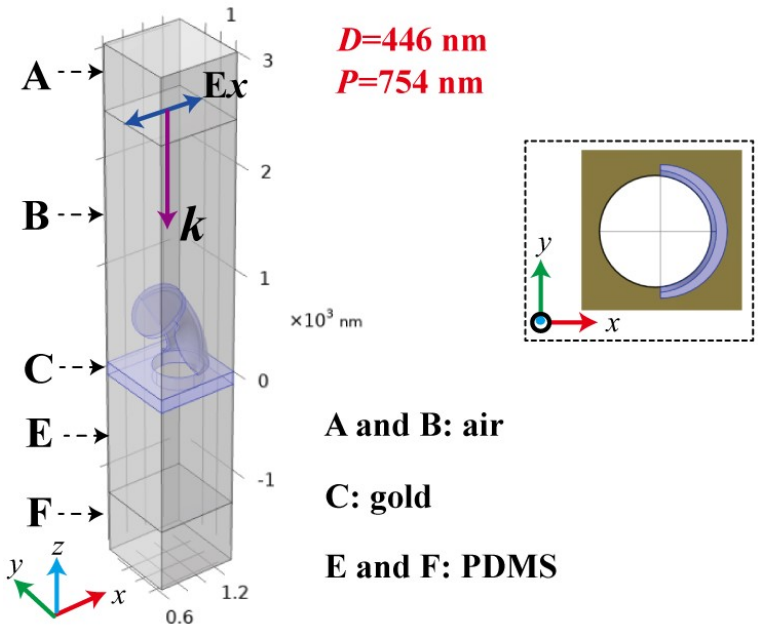

Fig. S10 Schematic showing an optical model with five regions, which are marked as "A, B, C, E and F", respectively. A and B represent the air. C is a curved freestanding hollow cylinder with the diameter *D*=446 nm and period *p*=754 nm. E and F refer to a PDMS substrate. The incident plane wave was a p-polarized wave whose electric field parallels the *x*-direction. The blue area of right inset represents a *xy* cross-section of the sidewall at z=0. The maximum and minimum widths of cross-section are 42 and 30 nm, respectively.

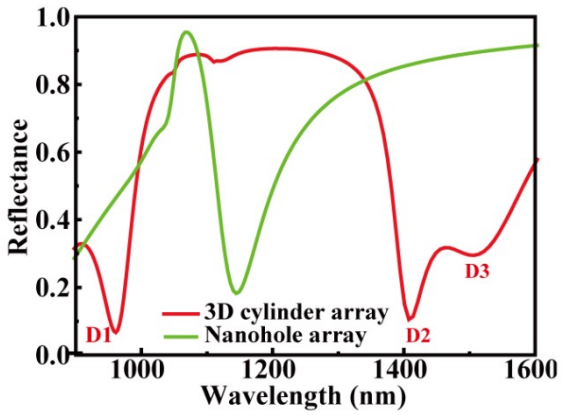

Fig. S11 Simulated reflectance spectra of a 3D freestanding hollow cylinder array (D=446 nm and *P*=754 nm) and corresponding nanohole array with a diameter of 446 nm.

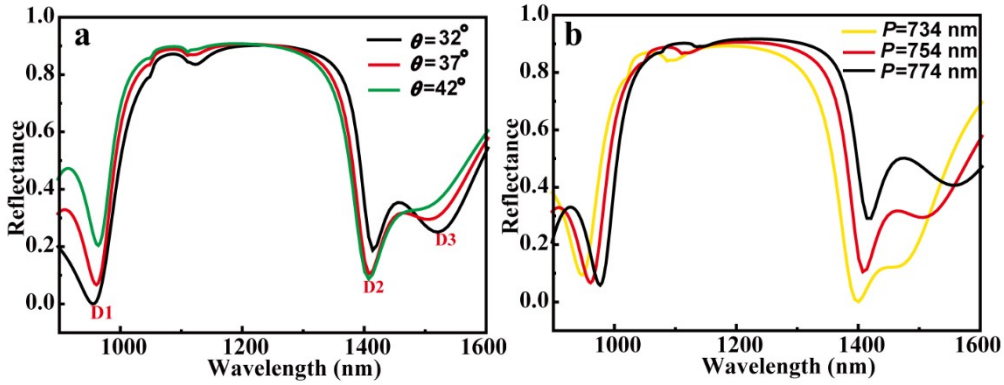

Fig. S12 Simulated reflectance spectra of the freestanding hollow cylinder arrays with a diameter of 446 nm as the functions of (a) the slant angle θ of the top-disc and (b) the period P.

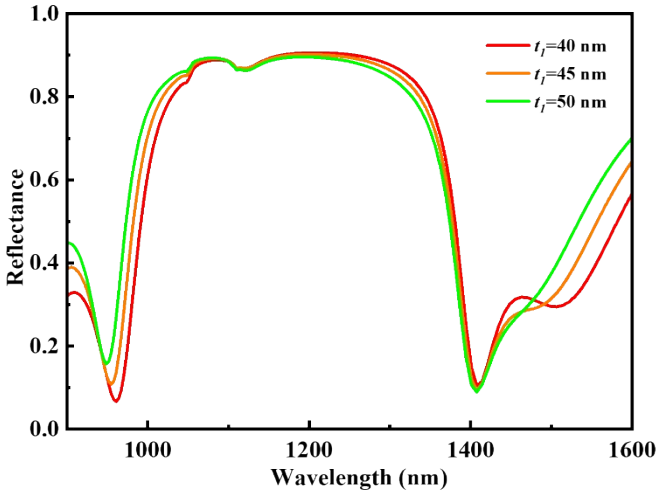

Fig. S13 Simulated reflectance spectra of the 3D curved freestanding cylinder array with a diameter of 446 nm for different thicknesses t_1 of the sidewall.

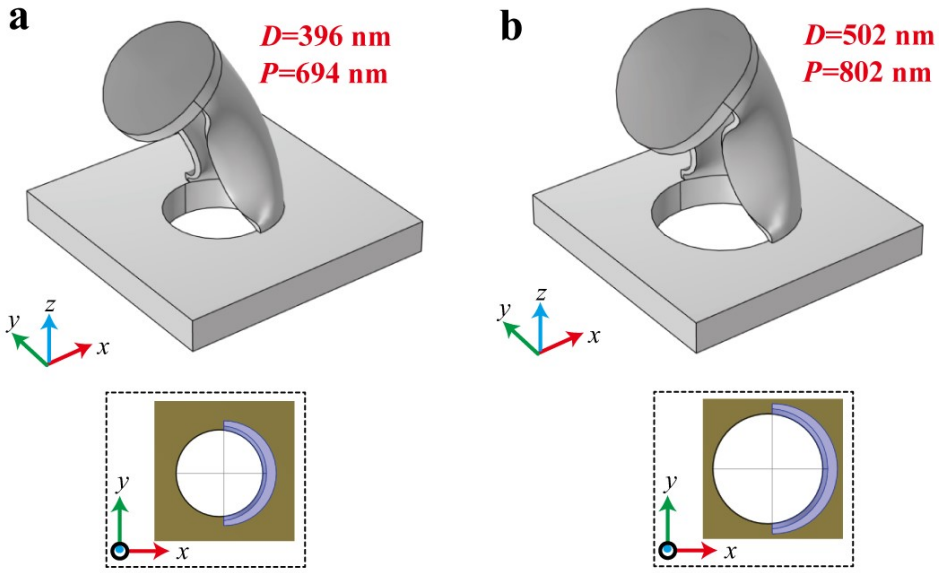

Fig. S14 (a-b) FEM simulation model of the 3D curved freestanding cylinders with the diameters (*D*=396 and 502 nm). The blue areas of right insets represent the *xy* cross-section of the sidewall at z=0. The maximum and minimum widths of cross-section are still 42 and 30 nm, respectively.

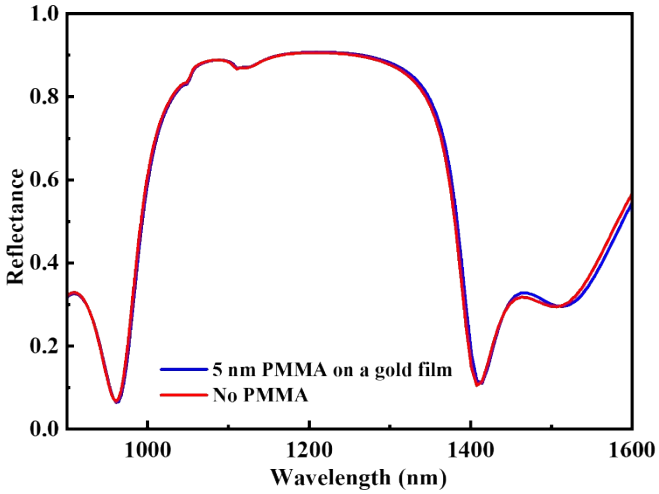

Fig. S15 Simulated reflectance spectrum of the 3D curved freestanding cylinder array with a diameter of 446 nm when it exhibits a 5 nm-thickness PMMA on the bottom gold film.